HHS Public Access

Author manuscript

AJR Am J Roentgenol. Author manuscript; available in PMC 2016 April 28.

Published in final edited form as:

AJR Am J Roentgenol. 2015 November ; 205(5): 1026–1037. doi:10.2214/AJR.14.14185.

Radiation Dose Reduction in Pediatric Body CT Using Iterative Reconstruction and a Novel Image-Based Denoising Method

Lifeng Yu[1], **Joel G. Fletcher**, **Maria Shiung**, **Kristen B. Thomas**, **Jane M. Matsumoto**, **Shannon N. Zingula**, and **Cynthia H. McCollough**

Department of Radiology, Mayo Clinic, 200 First St SW, Rochester, MN 55905

Abstract

OBJECTIVE—The objective of this study was to evaluate the radiation dose reduction potential of a novel image-based denoising technique in pediatric abdominopelvic and chest CT examinations and compare it with a commercial iterative reconstruction method.

MATERIALS AND METHODS—Data were retrospectively collected from 50 (25 abdominopelvic and 25 chest) clinically indicated pediatric CT examinations. For each examination, a validated noise-insertion tool was used to simulate half-dose data, which were reconstructed using filtered back-projection (FBP) and sinogram-affirmed iterative reconstruction (SAFIRE) methods. A newly developed denoising technique, adaptive nonlocal means (aNLM), was also applied. For each of the 50 patients, three pediatric radiologists evaluated four datasets: full dose plus FBP, half dose plus FBP, half dose plus SAFIRE, and half dose plus aNLM. For each examination, the order of preference for the four datasets was ranked. The organ-specific diagnosis and diagnostic confidence for five primary organs were recorded.

RESULTS—The mean (± SD) volume CT dose index for the full-dose scan was 5.3 ± 2.1 mGy for abdominopelvic examinations and 2.4 ± 1.1 mGy for chest examinations. For abdominopelvic examinations, there was no statistically significant difference between the half dose plus aNLM dataset and the full dose plus FBP dataset (3.6 ± 1.0 vs 3.6 ± 0.9, respectively; $p = 0.52$), and aNLM performed better than SAFIRE. For chest examinations, there was no statistically significant difference between the half dose plus SAFIRE and the full dose plus FBP (4.1 ± 0.6 vs 4.2 ± 0.6, respectively; $p = 0.67$), and SAFIRE performed better than aNLM. For all organs, there was more than 85% agreement in organ-specific diagnosis among the three half-dose configurations and the full dose plus FBP configuration.

CONCLUSION—Although a novel image-based denoising technique performed better than a commercial iterative reconstruction method in pediatric abdominopelvic CT examinations, it performed worse in pediatric chest CT examinations. A 50% dose reduction can be achieved while maintaining diagnostic quality.

Keywords

CT; CT protocol optimization; pediatric CT; radiation dose reduction

[1]Address correspondence to L. Yu (yu.lifeng@mayo.edu).

CT technology provides fast and high-quality images for the detection and staging of disease across the thoracoabdominal cavity of pediatric patients. However, because of concerns that the potential risk for radiation-induced malignancy in children is higher than that in adults [1-4], tremendous effort has been devoted to reducing radiation doses in pediatric CT examinations while maintaining diagnostic quality [5-10]. Radiation dose reduction, however, generally leads to an increase in image noise when other conditions are fixed. Many approaches have been developed for reducing noise in CT while maintaining spatial resolution to retain diagnostic-quality images. Iterative reconstruction (IR) techniques have received considerable attention because of their potential advantages over traditional filtered back-projection (FBP)–based reconstruction methods [11]. It has been shown that implementation of various IR techniques can reduce noise in reduced-dose scans in adult CT [9, 12–18] and pediatric CT examinations [19, 20].

One limitation of IR methods is that they are mostly available only on newer scanner models. A large number of relatively older scanners, which are still widely used in CT practice, do not have IR options, and upgrading equipment to IR-compatible platforms can be quite expensive. Even when an IR technique is offered as an upgrade, the performance may be suboptimal when compared with the performance achieved using newer scanners because of the limitations of the older scanner model or the older image reconstruction system.

In part to address the need for dose reduction on older scanners of various makes and models, we recently developed an image-based noise reduction method based on nonlocal means (NLM) filtering that is adapted to the local noise level in CT images [21]. The local noise level was estimated using an analytic model based on photon statistics and scanner geometry. We implemented this adaptive NLM (aNLM) denoising method on a workstation equipped with eight graphical processing units, to speed up the calculation, which can serve multiple CT systems from different vendors in a clinically acceptable time frame. The proposed aNLM denoising method has two main advantages over typical IR methods. First, because there is no need to access raw CT data, the aNLM denoising method can be implemented on any CT scanner as a postprocessing step. Second, the aNLM denoising method estimates the local noise level in the CT images during denoising, which provides an effective way to reduce noise throughout the imaging volume without sacrificing structural edge information.

The purpose of this study was to evaluate the image quality of the aNLM denoising method in both pediatric abdominopelvic and chest routine examinations performed for 50 patients and to compare its performance with that of a commercially available IR method and use of traditional FBP images.

Materials and Methods

Patients and CT Protocols

This study was approved by the institutional review board at Mayo Clinic in Rochester, Minnesota, and was compliant with HIPAA guidelines. The requirement for informed consent was waived for this retrospective study. From January 29, 2013, through September

16, 2013, data from clinically indicated pediatric body CT examinations were collected. Radiologists reviewed these cases and selected 50 (25 abdominopelvic and 25 chest cases) for evaluation. The inclusion criteria were as follows: patient age younger than 18 years, use of size-appropriate scanning protocols, and archived CT projection data.

All 50 examinations were acquired using clinically implemented routine pediatric CT protocols, which were derived from previously developed weight-based technique charts using size-based kilovoltage selection and automatic exposure control [8, 22] (Table 1). Examinations were performed using a Definition Flash CT system (Siemens Healthcare). CT projection data were archived. The Quality Reference mAs setting (Siemens Healthcare) in these protocols, which is the effective tube current–exposure time product considered to yield an acceptable image quality for a reference-size patient, was increased substantially compared with that in Yu et al. [22], to account for a change in the reference patient size made by the manufacturer. The reference patient size for pediatric protocols, which was a 5-year-old pediatric patient with a body weight of 20 kg in previous automatic exposure control software, was changed to an adult patient with a body weight of 75 kg.

Low-Dose Simulation, Image Reconstruction, and Denoising

Using a validated low-dose simulation tool that takes into account automatic exposure control system behavior, the bowtie filter, and detector electronic noise [23], we simulated images with 50% of the original dose level for all 50 examinations. Phantom experiments showed that the simulated noise matched that of actual reduced-dose phantom measurements. Noise spatial correlation was also verified as appropriate with the use of a noise power spectrum analysis [23].

For each of the 50 cases, projection CT data corresponding to the full dose and the half dose were loaded onto the scanner, and three different reconstructions were performed: full dose plus FBP using a medium sharp kernel (i.e., the B40 kernel); half dose plus FBP, also with use of the B40 kernel; and half dose plus IR, with use of a medium sharp iterative kernel I30 with a strength setting of 3 (i.e., I30–3). The commercially available IR technique that was used is referred to as sinogram-affirmed iterative reconstruction (SAFIRE, Siemens Healthcare). The image thickness and reconstruction interval were each 3 mm. The I30–3 setting for SAFIRE was based on the recommendation of the American Association of Physicists in Medicine for chest and abdominopelvic CT examinations of adult patients

The fourth image dataset was created by sending the half dose plus FBP images to a workstation for noise reduction with use of the aNLM method. The denoising parameter of the aNLM method was selected using a small pilot study involving six cases (two abdominopelvic and four chest cases) such that the noise reduction associated with aNLM was roughly matched to that associated with SAFIRE. A pediatric radiologist was asked to rate her preference between the SAFIRE and aNLM denoised images. Through this small pilot study, we confirmed that the image quality obtained with aNLM was at least very close to that obtained with SAFIRE for these six cases with the selected denoising strength before a formal large-scale evaluation was started. With four different image sets for each case, a total of 200 cases were evaluated by each of three observers.

Observer Study and Image Quality Evaluation

Three radiologists (all of whom subspecialized in pediatric radiology, with two having more than 10 years of experience and one having 3 years of experience) independently evaluated each volumetric dataset by use of a clinical computer workstation with dual monitors (Advantage Workstation 4.3, GE Healthcare). For each examination type, examinations were anonymized for each patient, dose level, and reconstruction type. The readers evaluated chest CT examinations separately from abdomino-pelvic examinations, with randomization of the sequence of the dose level and reconstruction method. Although readers were blinded to reconstruction and dose parameters, they were required to pan up and down through the datasets to evaluate overall image quality as well as organ-specific information, with use of a standardized data sheet (Appendix 1). They were instructed to change window settings as they would when interpreting routine clinical examinations. The clinical indication for each patient was provided before image evaluation.

For each examination, overall image quality was evaluated using a 5-point scale, with a score of 1 denoting an image considered to be non-diagnostic because of excessive noise, artifacts, or both; 2, an image of questionable use for diagnostic purposes because of excessive noise, artifacts, or both; 3, a diagnostic image with moderate but acceptable noise, artifacts, or both; 4, an image with mild noise but causing no change in diagnostic confidence; and 5, a routine diagnostic-quality image.

In addition, organ- or structure-specific questions were asked regarding the major structures. For chest CT examinations, the readers assigned lung and mediastinal findings a diagnostic code (with 0 denoting normal; 1, abnormal but cannot be characterized; and 2, abnormal but able to be characterized) and a diagnostic-quality image confidence score (with 1 denoting an image that is nondiagnostic and cannot identify or rule out lesion; 2, an image that will potentially miss lesions; 3, an image that will probably not miss or mischaracterize lesions; 4, an image that most likely will identify all abnormalities; and 5, an image that can detect lesions without diagnostic compromise). For abdominopelvic examinations, three primary organs (liver, kidney, and small bowel) were also evaluated using identical diagnosis codes and diagnostic-quality image scores. In addition, image sharpness was described for abdominopelvic CT images with use of a 5-point scale (with 1 denoting very sharp; 2, mildly un-sharp with no diagnostic difference; 3, moderately unsharp, resulting in questionable diagnostic difference; 4, noticeably blurry with poorly defined edges; and 5, nondiagnostic).

After evaluating the 100 CT examinations for each body part, the study coordinator provided instructions so the four corresponding datasets for each patient could be loaded onto the computer workstation for side-by-side comparison, which was also done in blinded fashion. Readers then ranked the dose plus reconstruction configurations in order of preference (with 1 denoting most preferred and 4 denoting least preferred).

Quantitative evaluation included measuring the mean (± SD) of the CT number in the midliver, midkidney, and bladder for abdominopelvic examinations and in the aortic arch, left ventricle, and hepatic dome for chest examinations. Anatomic structures were avoided

when placing the ROI. Measurements were made three times on adjacent slices and were averaged.

Data and Statistical Analysis

For each of the four configurations for abdominopelvic and chest examinations, the mean and SD of the overall image scores were calculated. These descriptive statistics were also provided for organ- and structure-specific diagnostic confidence scores and image sharpness scores (for abdomino-pelvic examinations). The difference in these parameters between each pair of configurations (full dose plus FBP vs half dose plus FBP, full dose plus FBP vs half dose plus IR, full dose plus FBP vs half dose plus aNLM, half dose plus FBP vs half dose plus IR, half dose plus FBP vs half dose plus aNLM, and half dose plus aNLM vs half dose plus IR) was tested using a Wilcoxon signed rank test (JMP version 9.0, SAS Institute). A statistically significant difference was denoted by $p < 0.05$. The test was performed for each individual reader and for all readers' data pooled together.

For organ- and structure-specific diagnostic codes, agreement between the full dose plus FBP evaluation and the half-dose configurations was calculated per reader for all half-dose configurations for all CT examinations. Agreement was calculated in two ways. First, the percentage of cases with absolute agreement between diagnosis scores was calculated. Second, normality agreement was calculated (i.e., the full-dose and the half-dose configuration both had to be normal, or both had to not be normal; the latter possibility was indicated by a diagnosis score of 1 or 2). For any reader, agreement of less than 80% was considered inferior agreement.

The mean and SD of the preference ranking scores were also calculated. The ranking scores from each reader and from all readers combined were compared for the four image sets.

The mean CT numbers and the noise in the IR and aNLM denoised images were compared with those in the original FBP images. The accuracy of the CT number was verified after noise reduction. The amount of noise reduction was quantified for both the IR and aNLM denoising methods.

Results

Patient Cohort

Twenty-five patients who underwent abdominopelvic CT examinations and 25 patients who underwent chest CT examinations were included in the study; of these patients, 18 patients in the abdominopelvic CT group and 12 patients in the chest CT group had a positive finding. Table 2 shows the age and scanning information (IV contrast agent status, kilovoltage, and volume CT dose index [$CTDI_{vol}$]) for patients who underwent abdominopelvic and chest CT examinations. The size-specific dose estimate was also reported [24].

Overall Image Quality

The overall image quality scores for abdominopelvic and chest CT examinations are shown in Figs. 1A and 1B, respectively. Detailed overall image quality scores for each reader and *p* values comparing each pair of the four datasets are provided in Appendix 2.

Abdominopelvic images—Both SAFIRE and aNLM significantly improved the overall image quality, compared with the half dose plus FBP ($p < 0.01$). The aNLM denoising method performed better than SAFIRE (3.61 ± 1.01 vs 3.33 ± 0.89, respectively; $p < 0.01$). The rated image quality in aNLM denoised images at half dose was comparable to that in the original full-dose images (3.61 ± 1.01 vs 3.55 ± 0.86, respectively; $p = 0.52$).

Chest images—SAFIRE significantly improved the overall image quality, compared with the half dose plus FBP ($p < 0.001$). Compared with the full dose plus FBP, SAFIRE fully restored the image quality at half dose (4.12 ± 0.61 for the half dose plus SAFIRE vs 4.16 ± 0.58 for the full dose plus FBP; $p = 0.67$). The aNLM method improves image quality, compared with the half dose plus FBP (3.68 ± 0.69 vs 3.40 ± 0.65, respectively; $p = 0.01$). However, the aNLM method was rated worse than both the full dose plus FBP ($p < 0.01$) and the half dose plus SAFIRE ($p < 0.01$).

Organ-Specific Diagnosis

For every examination, radiologists were asked to record organ-specific diagnosis codes along a 3-point scale (with 0 denoting normal; 1, abnormal but cannot be characterized; and 2 abnormal but can be characterized). For each reader and organ, the reference diagnosis code was the reader-specific diagnosis code given for the full dose plus FBP evaluation. The percentage agreement among the three half-dose configurations and the full dose plus FBP is provided in Tables 3 and 4. For each organ, both types of agreement (absolute agreement and normality agreement) are listed.

Abdominopelvic images—For the liver diagnosis code, there was exact agreement between full dose plus FBP and the half-dose configurations more than 88% of the time, except for one reader who had only 80% agreement for the half dose plus FBP. The percentage agreement for aNLM (93%) and SAFIRE (92%) was slightly higher than that for FBP (88%). Similar findings were found for the kidney diagnosis code, with one reader having only 76% agreement when evaluating half-dose SAFIRE. The percentage agreement for aNLM was the highest (97%). For the small-bowel diagnosis code, the absolute agreement was more than 85%, but one of the readers had only 72% agreement for half-dose FBP and SAFIRE and 83% agreement for aNLM. The percentage agreement for aNLM was again the highest (89%). After averaging across all three organs, the half dose plus aNLM had a better percentage agreement than did the half dose plus FBP and the half dose plus SAFIRE (93% vs 89% vs 89%, respectively). The agreement for normality showed the same trend, with agreement between 83% and 100% noted.

Chest images—For lung and mediastinal diagnoses, there was 80% or greater agreement for all readers between all of the half-dose configurations and each reader's full dose plus FBP reference diagnosis.

Organ Diagnostic Confidence Evaluation

Abdominopelvic images—The diagnostic confidence scores for all three organs (liver, kidney, and small bowel) showed trends similar to those noted for overall image quality scores. There were no statistically significant differences between the half dose plus aNLM and the full dose plus FBP images for the liver (3.83 ± 1.11 vs 3.97 ± 0.9, respectively; p= 0.23) and kidney (4.05 ± 0.97 vs 4.23 ± 0.76, respectively; p = 0.16). There was a weakly statistically significant difference between the half dose plus aNLM and the full dose plus FBP images for the small bowel (3.77 ± 0.95 vs 3.99 ± 0.66, respectively; p = 0.044), when all readers were considered; however, for two of three readers, the difference was not statistically significant (p= 0.84 and p= 0.56). The performance of SAFIRE was statistically significantly worse than that of aNLM denoising, for all three abdominopelvic organs (p= 0.03, p= 0.049, and p< 0.01, respectively).

Chest images—The diagnostic confidence scores for both the lung and the mediastinum showed a trend similar to that noted for overall image quality scores. There was no statistically significant difference between half dose plus SAFIRE and full dose plus FBP images for the lung (4.36 ± 0.60 vs 4.36 ± 0.61, respectively; p = 1.0) and mediastinum (4.49 ± 0.54 vs 4.51 ± 0.50, respectively; p = 0.83). The performance of SAFIRE was slightly but statistically significantly higher than that of aNLM denoising for both organs (4.36 ± 0.60 vs 4.13 ± 0.74, respectively, for the lung vs 4.49 ± 0.54 vs 4.27 ± 0.69, respectively, for the mediastinum; p <0.01).

The organ- and structure-specific diagnostic confidence scores for each structure, for each reader, site, and configuration (dose plus reconstruction), are shown in Appendix 2.

CT Image Sharpness

There was no loss of sharpness of images from abdominopelvic CT examinations conducted with both SAFIRE and aNLM denoising, compared with images for which the original full-dose configuration was used (SAFIRE, 2.51 ± 1.06; aNLM, 2.27 ± 1.04; original full dose, 2.29 ± 0.80), with aNLM being almost identical to the original full dose (p = 0.80).

Of interest, the sharpness of images obtained with the half dose plus FBP was quite low, potentially because of the poor impression of the noisy images. The image sharpness of the chest CT examinations was not evaluated. The results are expected to be similar to those noted in the abdominopelvic CT examinations.

Preference Testing

The ranking order of the four configurations used for the three abdominopelvic organs (liver, kidney, and bladder) is shown in Figs. 2A–2C, respectively. The ranking order for the two chest organs (lung and mediastinum) is shown in Figs. 3A and 3B, respectively.

Abdominopelvic images—Readers 1 and 3 ranked image quality consistently for all three organs, with the configurations ranked from most to least preferred as follows: half dose plus aNLM, half dose plus SAFIRE, full dose plus FBP, and half dose plus FBP. Reader 2 had a slightly different ranking. She also preferred the half dose plus aNLM

method for the liver and kidney but ranked it third behind full dose plus FBP and half plus dose SAFIRE for the small bowel. Figure 4 shows a comparison of the use of the four configurations for abdominopelvic cases.

Chest images—Regarding the quality of CT images of the mediastinum, all three readers had the same ranking order for the four configurations. This ranking, from most to least preferred configuration, was as follows: half dose plus SAFIRE, full dose plus FBP, half dose plus aNLM, and half dose plus FBP. For the quality of CT images of the lung, the ranking order of readers 1 and 3 was the same as that for the mediastinum, whereas reader 2 had a slightly different ranking: full dose plus FBP, half dose plus SAFIRE, half dose plus aNLM, and half dose plus FBP. Figure 5 shows the four image sets representing use of the four configurations for a representative chest examination.

CT Number and Noise

The mean noise of the half dose plus FBP was 40.4% and 47.8% higher than that of the full dose plus FBP images in chest and abdominopelvic examinations, respectively. These findings are consistent with the relationship between noise and radiation dose, as determined by the inverse square root law. Both the half dose plus SAFIRE and the half dose plus aNLM decreased image noise substantially, compared with half dose plus FBP images (for SAFIRE, by 40.4% ± 5.4% [for chest CT] and by 42.0% ± 2.8% [for abdominopelvic CT]; for aNLM, by 32.0% ± 11.9% [for chest CT] and by 47.8% ± 6.9% [for abdominopelvic CT]). The CT number did not change substantially after applying noise reduction; the mean difference in CT number was 0.3 HU (95% CI, −0.1 to 0.6 HU) for SAFIRE and −1.5 HU (95% CI, −2.0 to −1.0) for aNLM, compared with the original images.

Discussion

On the basis of the results of this study, we expect that, with use of the proposed aNLM denoising method for abdominopelvic examinations or with use of the commercially available SAFIRE method for chest examinations, a dose reduction of at least 50% can be achieved in pediatric CT examinations without sacrificing the diagnostic value of the image, reducing potential risk of radiation-induced malignancy, particularly in young patients with cancer or chronic diseases, who will likely undergo repeat imaging examinations.

A true IR method typically reconstructs images by optimizing an objective function that includes both a fidelity term and a regularization term [11]. The fidelity term can incorporate x-ray photon statistics and physical factors such as x-ray source and detector geometry and x-ray beam spectra, which may improve the quantitative accuracy and spatial resolution. The regularization term is included in the objective function to reduce noise while maintaining edge information. Because of the long computational time in a true IR method (e.g., model-based iterative reconstruction from GE Healthcare), implementation in clinical practice is challenging. To speed up computation, various hybrid IR methods, such as SAFIRE (Siemens Healthcare), adaptive iterative dose reduction (AIDR3D, Toshiba), and iDose (Philips Healthcare), are now commercially available. Many clinical studies have also shown the potential for image quality improvement and radiation dose reduction with the use of these hybrid methods [9, 15-18].

NLM filtration denoises images by exploiting the inherent redundant information in regions nearby the pixel of interest [25]. A high degree of structural detail can be preserved while reducing the image noise. However, a global filtering setting is typically used in the standard NLM algorithm, which cannot achieve optimal performance in CT because the noise varies significantly throughout the 3D volume. In the evaluated aNLM technique, the noise level in different regions was analytically calculated on the basis of a model of photon statistics and system geometry, and the NLM algorithm was modified to adapt to this local noise level [21]. This modification makes use of the local noise information and can achieve optimal noise reduction throughout the imaging volume. The main advantage of aNLM denoising is that it is scanner independent and can be implemented on any scanner, whereas SAFIRE and other commercial products of IR are scanner dependent and are usually only available on newer scanners. The main disadvantage of the aNLM method is that it could add an additional 5–10 minutes to each examination.

Both aNLM and IR allow noise and dose reduction, but the amount of dose reduction that can be achieved without sacrificing diagnostic quality remains unclear in pediatric CT. Our results showed that both aNLM and SAFIRE improved image quality over the FBP method, with aNLM being better than SAFIRE in abdominopelvic examinations and slightly worse in chest examinations. Because of these results and other encouraging results from studies conducted to evaluate adult CT examinations [26], we have been implementing the aNLM de-noising method for relatively older scanners across our institution’s CT practice.

Using lower tube potentials is a useful approach to reducing radiation dose, especially in pediatric CT examinations [27-29]. Although pediatric patients are rarely large enough to prohibit 80-kV scanning [30, 31], most current CT systems are limited in the amount of tube current that can be delivered to achieve a reasonably fast scanning speed, which is often critical in pediatric CT. Thus, scanning speed may be sacrificed to achieve sufficient radiation output; otherwise, the image noise will increase substantially, which diminishes the examination quality and reader confidence. The tube potential technique chart in Table 1, which was the starting point for our image quality and radiation dose evaluation, was a result of evaluation considering both image quality and scanning speed [8, 22].

We performed an evaluation of the organ-specific diagnostic agreement between images obtained with the reduced dose and the full dose, in addition to subjective image quality scores. This evaluation was not a direct test of diagnostic performance. However, it is interesting to note that the organ-specific diagnostic agreement, especially the normality agreement, was not very different among all reconstruction and dose settings. These results implied that the diagnostic performance might not differ much among all evaluated settings, although the denoising and IR helped improve the perception of the images.

This study has some limitations. First, this is a retrospective study in which half-dose examinations were simulated using noise insertion software rather than by prospectively acquiring half-dose examinations of patients. Reduced-dose simulation is an efficient and safe approach to evaluate how low the radiation dose can go [32, 33]. The simulation software used in this study was developed in our institute and has been shown to be an accurate tool using both phantom and patient studies [23, 34, 35]. Second, primarily

subjective evaluation by pediatric radiologists was used in this study to determine the image quality score. A more strict evaluation should involve assessing diagnostic performance for a very specific task. This is a subject of our ongoing research to evaluate the same image-based aNLM denoising software for use in adult CT examinations [26]. Because our present study was limited by the number of patient examinations with similar positive findings, a diagnostic performance evaluation (e.g., sensitivity and specificity analysis) was not included in the current study. However, the dose reduction results derived from the current study have been implemented in our practice since July 2014 and have been accepted by all of our pediatric radiologists, which indicates that the evaluation conducted in this study is sufficiently accurate.

Conclusion

The use of a novel image-based denoising technique in pediatric abdominopelvic CT examinations and an IR technique in pediatric chest CT examinations resulted in a 50% radiation dose reduction while maintaining clinically acceptable image quality. Our novel denoising method, aNLM, performed better than the commercial IR method, SAFIRE, in abdominopelvic examinations, but it performed worse in chest examinations. Both, however, performed superiorly to the half dose plus FBP images.

Acknowledgments

We thank Armando Manduca, Dan Blezek, and Zhoubo Li for their contribution to the development and implementation of the adaptive nonlocal means technique.

Supported by a grant from the Thrasher Research Fund.

J. G. Fletcher and C. H. McCollough receive research support from Siemens Healthcare.

Appendix

Image Quality Evaluation Sheet - ABDOMEN/PELVIS

Patient ID:
Indication for exam:
Contrast:

	Overall Image Quality
1	Non-diagnostic due to excessive noise/artifacts
2	Diagnosis questionable due to excessive noise/artifacts
3	Diagnostic with moderate but acceptable noise/artifacts
4	Mild noise, no change of diagnostic confidence
5	Routine diagnostic image quality

Overall IQ score:

Abdomen/Pelvis 1 2 3 4 5

	Image Sharpness
1	Very sharp
2	Mildly un-sharp edges, no diagnostic difference
3	Moderately un-sharp, questionable diagnostic difference
4	Noticeable blur, poorly defined edges
5	Non-diagnostic

Image Sharpness:

Abdomen/Pelvis 1 2 3 4 5

Organ Evaluation and Diagnostic Confidence

Organ evaluation			Diagnostic Confidence	
0	Normal		1	Non-diagnostic, cannot identify or rule out lesion
1	abnormal but cannot characterize		2	Will potentially miss lesions
2	abnormal but can characterize		3	Will probably not miss or mischaracterize lesions
			4	Most likely will identify all abnormalities
			5	Can detect lesions without diagnostic compromise

		Organ evaluation	Diagnostic Confidence
Abdomen	Liver	0 1 2 NA	1 2 3 4 5 NA
	Kidney	0 1 2 NA	1 2 3 4 5 NA
Pelvis	Small Bowel	0 1 2 NA	1 2 3 4 5 NA

Comments:

APPENDIX 1.

Clinical Data Sheet Used by Pediatric Radiologists Assessing Abdominopelvic Image Quality.

Note—ID = identification, IQ = image quality, NA = not available.

APPENDIX 2

Overall Image Quality Score for Abdominopelvic and Chest CT Examinations and Diagnostic Confidence for Four Dose Plus Reconstruction Settings Used in CT Examinations of the Liver, Kidney, Small Bowel, Lung, and Mediastinum

Finding, Structure or Organ, Reader	Full Dose Plus FBP, Mean ± SD	Half Dose Plus FBP, Mean ± SD	Half Dose Plus SAFIRE, Mean ± SD	Half Dose Plus aNLM, Mean ± SD	*p*				
					Full Dose Plus FBP vs Half Dose Plus FBP	Full Dose Plus FBP vs Half Dose Plus SAFIRE	Full Dose Plus FBP vs Half Dose Plus aNLM	Half Dose Plus FBP vs Half Dose Plus SAFIRE	
Overall image quality–abdominopelvis									
Reader 1	3.36 ± 1.04	2.08 ± 0.86	3.16 ± 0.94	3.32 ± 1.03	< 0.01	0.39	0.79	< 0.01	<
Reader 2	3.32 ± 0.69	2.76 ± 0.72	2.96 ± 0.61	3.20 ± 0.76	< 0.01	0.06	0.55	0.27	
Reader 3	3.96 ± 0.68	2.92 ± 0.76	3.88 ± 0.83	4.32 ± 0.85	< 0.01	0.83	0.09	< 0.01	<
All readers	3.55 ± 0.86	2.59 ± 0.86	3.33 ± 0.89	3.61 ± 1.01	< 0.01	0.07	0.52	< 0.01	<
Diagnostic confidence–liver									
Reader 1	3.60 ± 1.04	1.96 ± 0.98	3.40 ± 1.08	3.44 ± 1.26	< 0.01	0.30	0.64	< 0.01	<
Reader 2	4.00 ± 0.82	3.24 ± 0.88	3.40 ± 1.08	3.60 ± 1.04	< 0.01	< 0.01	0.01	0.43	
Reader 3	4.32 ± 0.69	3.24 ± 0.88	4.00 ± 0.91	4.44 ± 0.71	< 0.01	0.21	0.64	< 0.01	<
All readers	3.97 ± 0.90	2.81 ± 1.09	3.60 ± 1.05	3.83 ± 1.11	< 0.01	< 0.01	0.23	< 0.01	<
Diagnostic confidence–kidney									
Reader 1	4.00 ± 0.87	2.40 ± 1.15	3.84 ± 0.85	3.88 ± 1.20	< 0.001	0.48	0.73	< 0.01	<
Reader 2	4.28 ± 0.68	3.48 ± 0.71	3.56 ± 0.82	3.84 ± 0.85	< 0.001	< 0.001	0.02	0.77	
Reader 3	4.40 ± 0.71	3.28 ± 0.94	4.20 ± 0.87	4.44 ± 0.71	< 0.001	0.45	0.97	< 0.01	<
All readers	4.23 ± 0.76	3.05 ± 1.05	3.87 ± 0.88	4.05 ± 0.97	< 0.001	< 0.01	0.16	< 0.01	<
Diagnostic confidence–small bowel									
Reader 1	3.72 ± 1.02	2.40 ± 1.08	3.56 ± 1.12	3.68 ± 1.25	< 0.001	0.51	0.84	< 0.01	<
Reader 2	3.84 ± 0.75	3.08 ± 0.93	3.20 ± 1.04	3.40 ± 0.96	< 0.001	< 0.01	< 0.01	0.79	
Reader 3	4.40 ± 0.71	3.24 ± 0.93	3.92 ± 1.08	4.33 ± 0.96	< 0.001	0.09	0.56	< 0.01	<
All readers	3.99 ± 0.66	2.92 ± 0.83	3.56 ± 0.93	3.77 ± 0.95	< 0.001	< 0.01	0.044	< 0.01	<
Overall image quality–chest									
Reader 1	4.32 ± 0.75	3.36 ± 0.70	4.32 ± 0.80	3.80 ± 0.82	< 0.01	1.00	< 0.01	< 0.01	
Reader 2	3.64 ± 0.86	3.24 ± 0.83	3.56 ± 0.92	3.44 ± 0.77	0.03	0.83	0.31	0.10	
Reader 3	4.52 ± 0.58	3.60 ± 0.76	4.48 ± 0.77	3.80 ± 1.00	< 0.01	1.00	< 0.01	< 0.01	
All readers	4.16 ± 0.58	3.40 ± 0.65	4.12 ± 0.61	3.68 ± 0.69	< 0.01	0.67	< 0.01	< 0.01	
Diagnostic confidence–lung									
Reader 1	4.68 ± 0.63	4.16 ± 0.90	4.68 ± 0.63	4.56 ± 0.82	< 0.01	1.00	0.45	< 0.01	
Reader 2	3.60 ± 1.00	3.40 ± 0.96	3.64 ± 1.08	3.44 ± 0.96	0.27	0.88	0.46	0.35	
Reader 3	4.80 ± 0.50	4.24 ± 0.93	4.76 ± 0.52	4.40 ± 0.82	< 0.01	1.00	< 0.01	< 0.01	
All readers	4.36 ± 0.61	3.93 ± 0.76	4.36 ± 0.60	4.13 ± 0.74	< 0.01	1.00	< 0.01	< 0.01	
Diagnostic confidence–mediastinum									

Finding, Structure or Organ, Reader	Full Dose Plus FBP, Mean ± SD	Half Dose Plus FBP, Mean ± SD	Half Dose Plus SAFIRE, Mean ± SD	Half Dose Plus aNLM, Mean ± SD	*p*				
					Full Dose Plus FBP vs Half Dose Plus FBP	Full Dose Plus FBP vs Half Dose Plus SAFIRE	Full Dose Plus FBP vs Half Dose Plus aNLM	Half Dose Plus FBP vs Half Dose Plus SAFIRE	
Reader 1	4.92 ± 0.28	4.68 ± 0.69	4.92 ± 0.28	4.80 ± 0.58	0.11	1.00	0.50	0.06	
Reader 2	3.92 ± 0.86	3.64 ± 0.86	3.96 ± 1.02	3.76 ± 0.88	0.04	1.00	0.34	0.04	
Reader 3	4.68 ± 0.69	3.84 ± 0.94	4.60 ± 0.71	4.24 ± 0.97	< 0.01	0.69	< 0.01	< 0.01	
All readers	4.51 ± 0.50	4.05 ± 0.65	4.49 ± 0.54	4.27 ± 0.69	< 0.01	0.83	< 0.01	< 0.01	

Note—FBP = filtered back-projection, SAFIRE = sinogram-affirmed iterative reconstruction (SAFIRE, Siemens Healthcare), aNLM = adaptive nonlocal means.

References

1. Brenner D, Elliston C, Hall E, Berdon W. Estimated risks of radiation-induced fatal cancer from pediatric CT. AJR. 2001; 176:289–296. [PubMed: 11159059]
2. Brody AS, Frush DP, Huda W, Brent RL. American Academy of Pediatrics Section on Radiology. Radiation risk to children from computed tomography. Pediatrics. 2007; 120:677–682. [PubMed: 17766543]
3. Rice HE, Frush DP, Farmer D, Waldhausen JH. APSA Education Committee. Review of radiation risks from computed tomography: essentials for the pediatric surgeon. J Pediatr Surg . 2007; 42:603–607. [PubMed: 17448753]
4. Miglioretti DL, Johnson E, Williams A, et al. The use of computed tomography in pediatrics and the associated radiation exposure and estimated cancer risk. JAMA Pediatr. 2013; 167:700–707. [PubMed: 23754213]
5. Frush DP. Strategies of dose reduction. Pediatr Radiol. 2002; 32:293–297. [PubMed: 11956713]
6. Singh S, Kalra MK, Moore MA, et al. Dose reduction and compliance with pediatric CT protocols adapted to patient size, clinical indication, and number of prior studies. Radiology. 2009; 252:200–208. [PubMed: 19435938]
7. Strauss KJ, Goske MJ, Kaste SC, et al. Image gently: ten steps you can take to optimize image quality and lower CT dose for pediatric patients. AJR. 2010; 194:868–873. [PubMed: 20308484]
8. Yu L, Bruesewitz MR, Thomas KB, Fletcher JG, Kofler JM, McCollough CH. Optimal tube potential for radiation dose reduction in pediatric CT: principles, clinical implementations, and pitfalls. RadioGraphics. 2011; 31:835–848. [PubMed: 21571660]
9. Singh S, Kalra MK, Shenoy-Bhangle AS, et al. Radiation dose reduction with hybrid iterative reconstruction for pediatric CT. Radiology. 2012; 263:537–546. [PubMed: 22517962]
10. Siegel MJ, Hildebolt C, Bradley D. Effects of automated kilovoltage selection technology on contrast-enhanced pediatric CT and CT angiography. Radiology. 2013; 268:538–547. [PubMed: 23564712]
11. Thibault JB, Sauer KD, Bouman CA, Hsieh J. A three-dimensional statistical approach to improved image quality for multislice helical CT. Med Phys. 2007; 34:4526–4544. [PubMed: 18072519]
12. Katsura M, Matsuda I, Akahane M, et al. Model-based iterative reconstruction technique for radiation dose reduction in chest CT: comparison with the adaptive statistical iterative reconstruction technique. Eur Radiol. 2012; 22:1613–1623. [PubMed: 22538629]

13. Pickhardt PJ, Lubner MG, Kim DH, et al. Abdominal CT with model-based iterative reconstruction (MBIR): initial results of a prospective trial comparing ultralow-dose with standard-dose imaging. AJR. 2012; 199:1266–1274. [PubMed: 23169718]
14. Shuman WP, Chan KT, Busey JM, et al. Standard and reduced radiation dose liver CT images: adaptive statistical iterative reconstruction versus model-based iterative reconstruction—comparison of findings and image quality. Radiology. 2014; 273:793–676. [PubMed: 25170546]
15. Winklehner A, Karlo C, Puippe G, et al. Raw data-based iterative reconstruction in body CTA: evaluation of radiation dose saving potential. Eur Radiol. 2011; 21:2521–2526. [PubMed: 21822785]
16. Baumueller S, Winklehner A, Karlo C, et al. Low-dose CT of the lung: potential value of iterative reconstructions. Eur Radiol. 2012; 22:2597–2606. [PubMed: 22699873]
17. Remer EM, Herts BR, Primak A, et al. Detection of urolithiasis: comparison of 100% tube exposure images reconstructed with filtered back projection and 50% tube exposure images reconstructed with sinogram-affirmed iterative reconstruction. Radiology. 2014; 272:749–756. [PubMed: 24814177]
18. Yamashiro T, Miyara T, Honda O, et al. Adaptive iterative dose reduction using three dimensional processing (AIDR3D) improves chest CT image quality and reduces radiation exposure. PLoS ONE. 2014; 9:e105735. [PubMed: 25153797]
19. Miéville FA, Berteloot L, Grandjean A, et al. Model-based iterative reconstruction in pediatric chest CT: assessment of image quality in a prospective study of children with cystic fibrosis. Pediatr Radiol. 2013; 43:558–567. [PubMed: 23224105]
20. Smith EA, Dillman JR, Goodsitt MM, Christodoulou EG, Keshavarzi N, Strouse PJ. Model-based iterative reconstruction: effect on patient radiation dose and image quality in pediatric body CT. Radiology. 2014; 270:526–534. [PubMed: 24091359]
21. Li Z, Yu L, Trzasko JD, et al. Adaptive nonlocal means filtering based on local noise level for CT denoising. Med Phys. 2014; 41:011908. [PubMed: 24387516]
22. Yu, L.; Fletcher, JG.; Thomas, K., et al. RSNA 2011. Oak Brook, IL: Radiological Society of North America; 2011. Optimization of pediatric body CT scanning protocols using a low dose simulation tool. (abstract) archive.rsna.org/2011/11008210.html [July 27, 2015]
23. Yu L, Shiung M, Jondal D, McCollough CH. Development and validation of a practical lower-dose-simulation tool for optimizing computed tomography scan protocols. J Comput Assist Tomogr. 2012; 36:477–487. [PubMed: 22805680]
24. American Association of Physicists in Medicine (AAPM). [July 23, 2015] AAPM Report No. 204: size-specific dose estimates (SSDE) in pediatric and adult body CT examinations. AAPM website. www.aapm.org/pubs/reports/RPT_204.pdf. Published 2011
25. Buades A, Coll B, Morel JM. A review of image denoising algorithms, with a new one. Multiscale Model Simul. 2005; 4:490–530.
26. Fletcher JG, Yu L, Li Z, et al. Observer performance in the detection and classification of malignant hepatic nodules and masses with CT image-space denoising and iterative reconstruction. Radiology. 2015; 276:465–478. [PubMed: 26020436]
27. Siegel MJ, Schmidt B, Bradley D, Suess C, Hildebolt C. Radiation dose and image quality in pediatric CT: effect of technical factors and phantom size and shape. Radiology. 2004; 233:515–522. [PubMed: 15358847]
28. Frush DP. Pediatric abdominal CT angiography. Pediatr Radiol. 2008; 38(suppl 2):S259–S266. [PubMed: 18401623]
29. Macdougall RD, Strauss KJ, Lee EY. Managing radiation dose from thoracic multidetector computed tomography in pediatric patients: background, current issues, and recommendations. Radiol Clin North Am. 2013; 51:743–760. [PubMed: 23830796]
30. Guimarães LS, Fletcher JG, Harmsen WS, et al. Appropriate patient selection at abdominal dual-energy CT using 80 kV: relationship between patient size, image noise, and image quality. Radiology. 2010; 257:732–742. [PubMed: 20959540]
31. Yu L, Li H, Fletcher JG, McCollough CH. Automatic selection of tube potential for radiation dose reduction in CT: a general strategy. Med Phys. 2010; 37:234–243. [PubMed: 20175486]

32. Mayo JR, Whittall KP, Leung AN, et al. Simulated dose reduction in conventional chest CT: validation study. Radiology. 1997; 202:453–457. [PubMed: 9015073]

33. Frush DP, Slack CC, Hollingsworth CL, et al. Computer-simulated radiation dose reduction for abdominal multidetector CT of pediatric patients. AJR. 2002; 179:1107–1113. [PubMed: 12388482]

34. Apel A, Fletcher JG, Fidler JL, et al. Pilot multireader study demonstrating potential for dose reduction in dual energy hepatic CT using non-linear blending of mixed kV image datasets. Eur Radiol. 2011; 21:644–652. [PubMed: 20878523]

35. Gabriel S, Eckel LJ, DeLone DR, et al. Pilot study of radiation dose reduction for pediatric head CT in evaluation of ventricular size. AJNR. 2014; 25:2237–2242. [PubMed: 25082822]

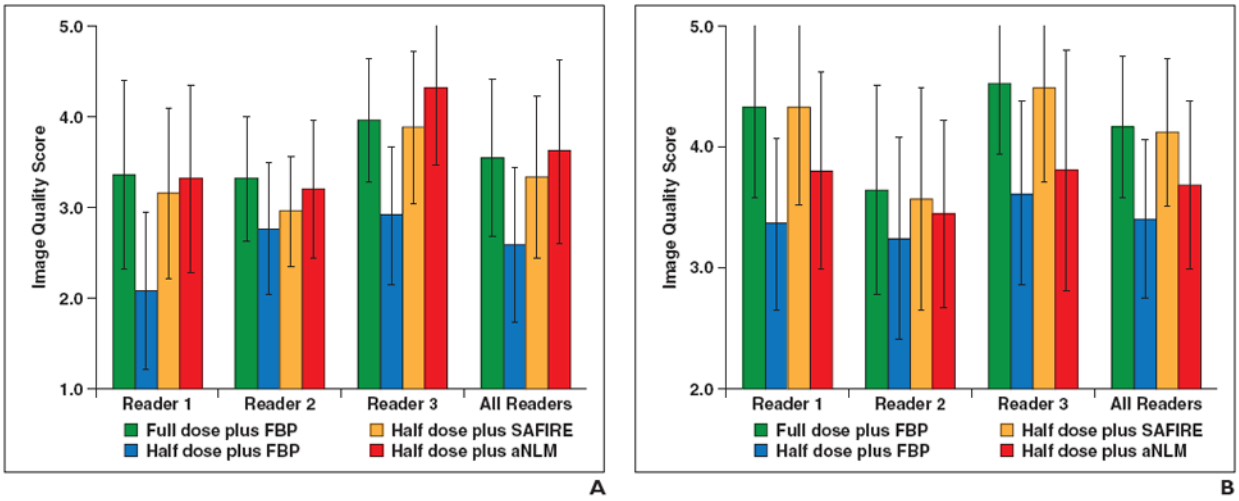

Fig. 1.

Overall image quality scores.

A and **B,** Graphs show image quality scores for abdominopelvic (**A**) and chest (**B**) CT examinations. FBP = filtered back-projection, SAFIRE = sinogram-affirmed iterative reconstruction (Siemens Healthcare), aNLM = adaptive nonlocal means.

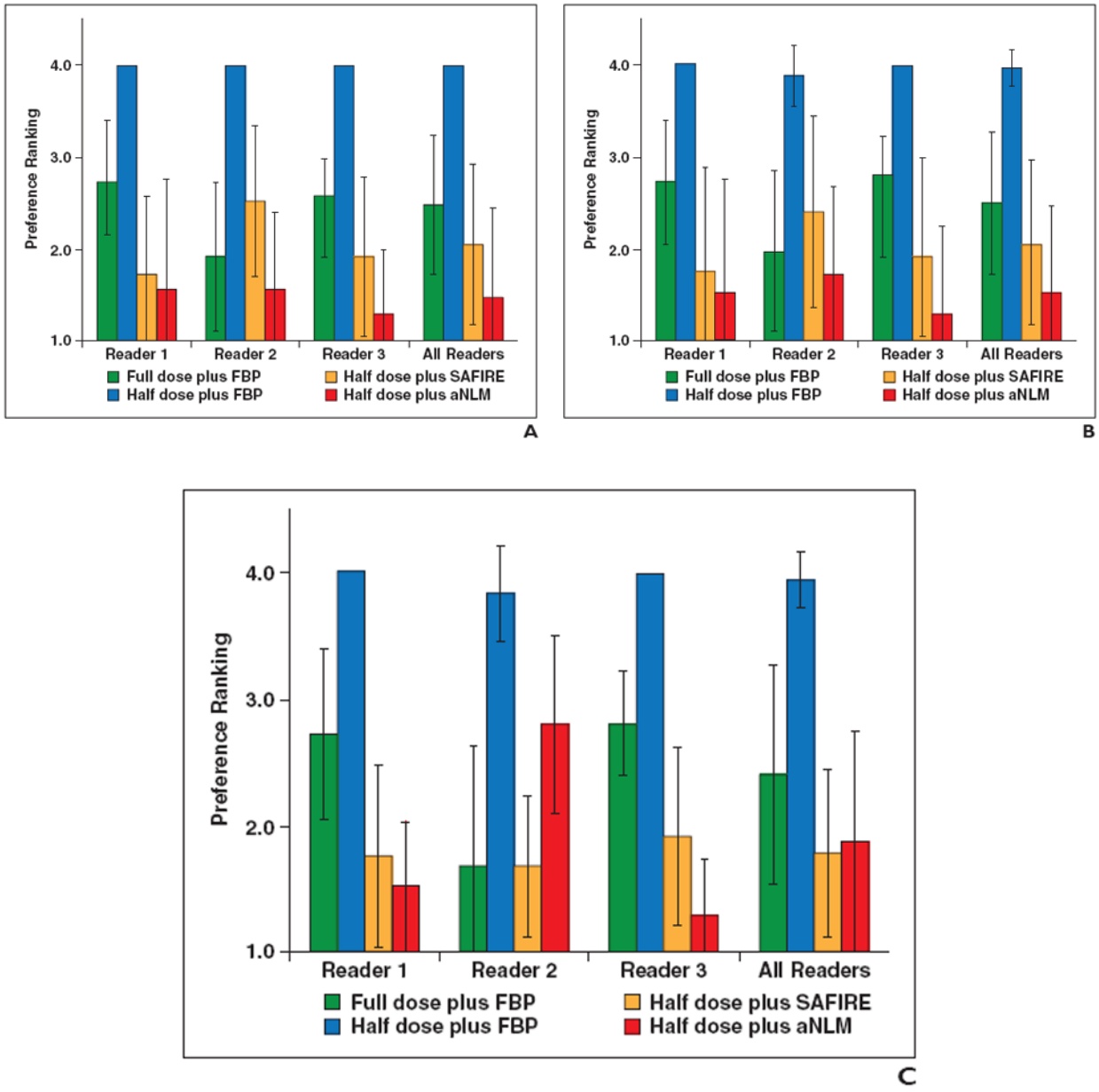

Fig. 2.

Preference ranking scores for liver, kidney, and small bowel.

A–C, Graphs show preference ranking scores for four configurations used in CT examinations of liver (**A**), kidney (**B**), and small bowel (**C**). FBP = filtered back-projection, SAFIRE = sinogram-affirmed iterative reconstruction (Siemens Healthcare), aNLM = adaptive nonlocal means.

A–C, Graphs show preference ranking scores for four configurations used in CT examinations of liver (**A**), kidney (**B**), and small bowel (**C**) FBP = filtered back-projection, SAFIRE = sinogram-affirmed iterative reconstruction (Siemens Healthcare), aNLM = adaptive nonlocal means.

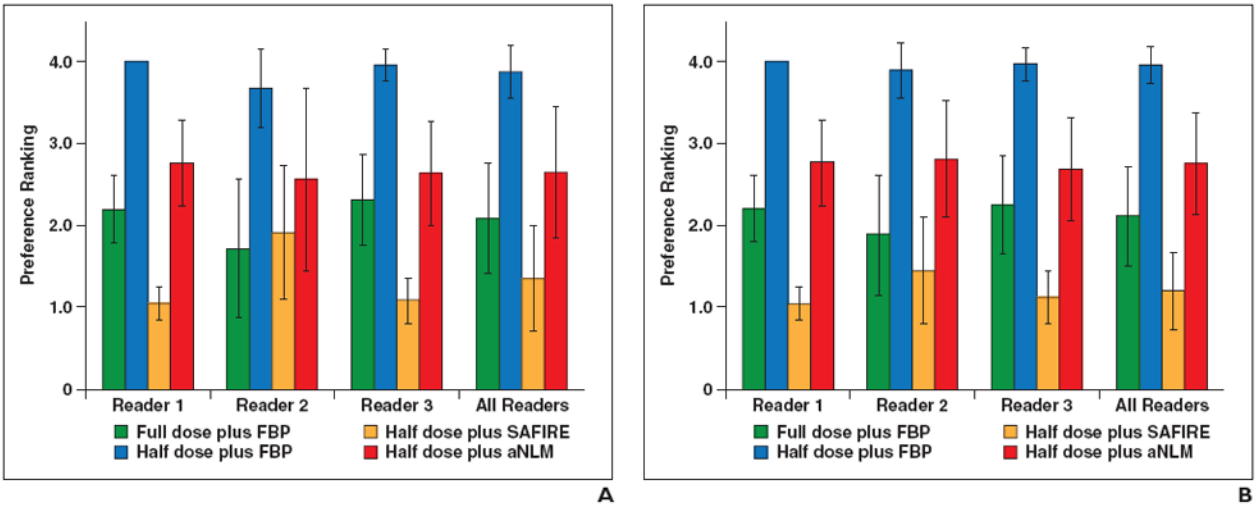

Fig. 3.

Preference ranking scores for lung and mediastinum.

A and **B,** Graphs show preference ranking scores for four configurations used for CT examinations of lung (**A**) and mediastinum (**B**). FBP = filtered back-projection, SAFIRE = sinogram-affirmed iterative reconstruction (Siemens Healthcare), aNLM = adaptive nonlocal means.

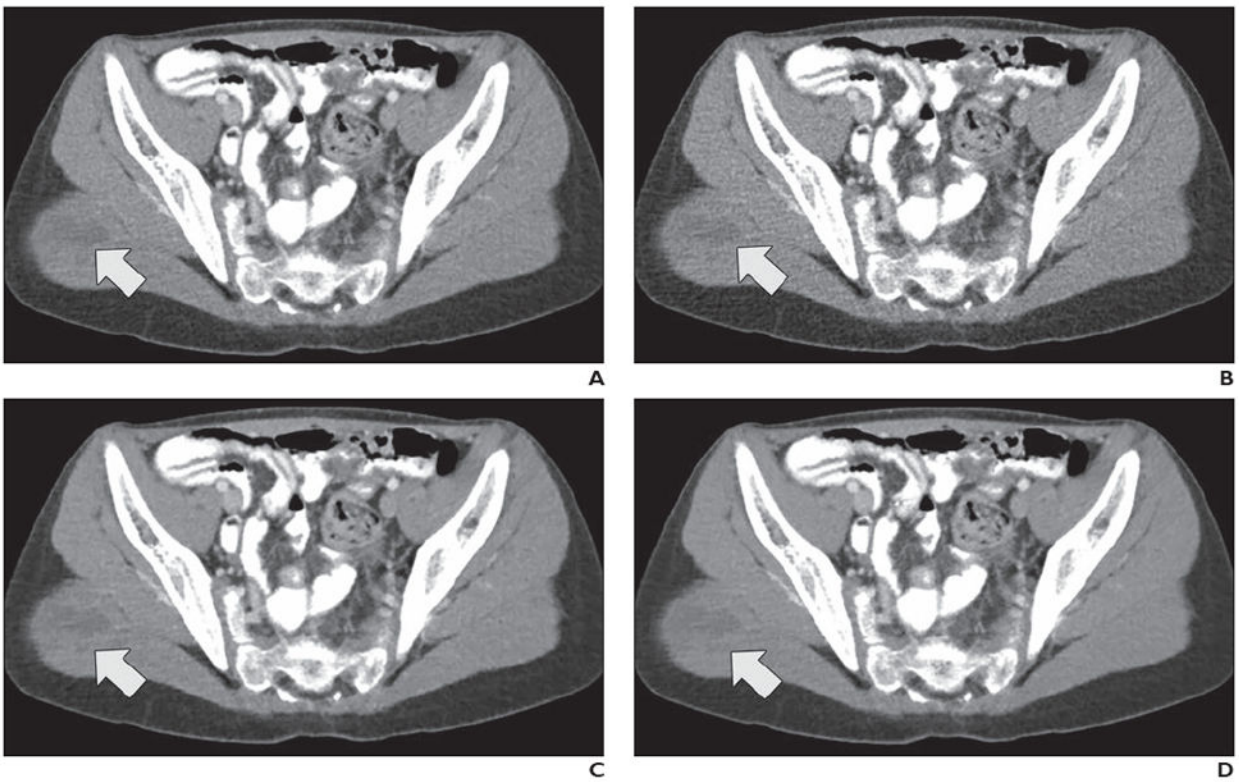

Fig. 4.

12-year-old boy with metastatic Wilms tumor in right gluteal muscle (*arrow*). After undergoing left nephrectomy for resection of Wilms tumor, patient underwent contrast-enhanced abdominopelvic CT performed to evaluate postoperative changes.

A–D, CT images shown compare four dose plus reconstruction settings: full dose plus filtered back-projection (FBP) (**A**), half dose plus FBP (**B**), half dose plus sinogram-affirmed iterative reconstruction (SAFIRE, Siemens Healthcare) (**C**), and half dose plus adaptive nonlocal means (aNLM) (**D**). Scanning parameters included kilovoltage of 120 kV and full-dose volume CT dose index of 5.8 mGy. Half dose was 2.9 mGy. All three readers ranked half dose plus aNLM images higher than original full-dose images. Average scores from all three readers for four images were as follows: 4.3 for full dose plus FBP, 3.0 for half dose plus FBP, 4.0 for half dose plus SAFIRE, and 4.3 for half dose plus aNLM.

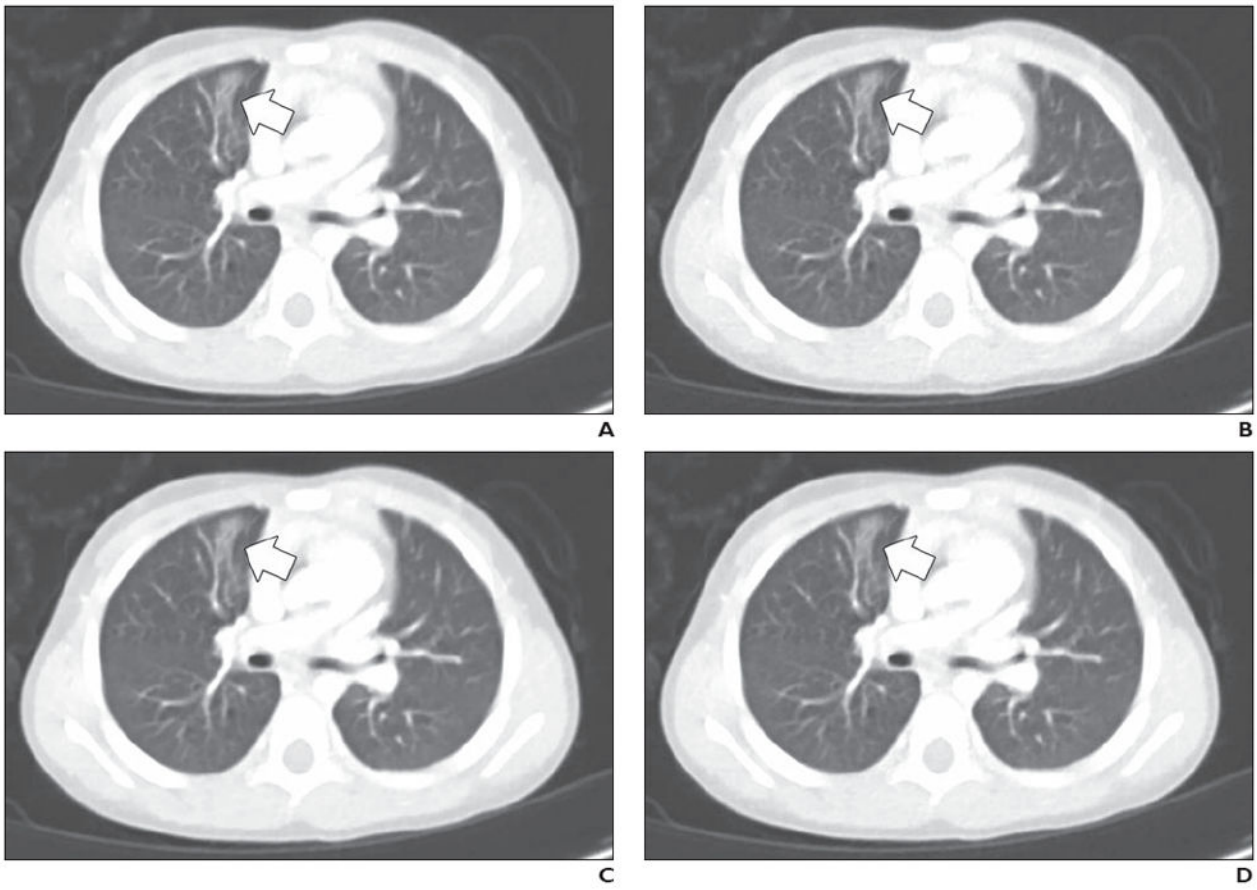

Fig. 5.

3-year-old girl with atelectasis in right upper lobe medially (*arrow*).

A–D, Contrast-enhanced chest CT images shown compare four dose plus reconstruction settings: full dose plus filtered back-projection (FBP) (**A**), half dose plus FBP (**B**), half dose plus sinogram-affirmed iterative reconstruction (SAFIRE, Siemens Healthcare) (**C**), and half dose plus adaptive nonlocal means (aNLM) (**D**). Scanning parameters included kilovoltage of 100 kV and full-dose volume CT dose index of 2.2 mGy. Half dose was 1.1 mGy. Average scores from all three readers for four images were as follows: 3.7 for full dose plus FBP, 3.0 for half dose plus FBP, 3.7 for half dose plus SAFIRE, and 4.3 for half dose plus aNLM.

TABLE 1

Protocols for Routine Pediatric Abdominopelvic and Chest CT Examinations

CT Examination Protocol, Contrast Agent Status, Patient Weight	Kilovoltage	Quality Reference Tube Current–Exposure Time Product (mAs)	Pitch	Rotation Time (s)	Collimation (mm)	Kernel	Thickness (mm)/Interval (mm)	$CTDI_{vol}$ (mGy)
Abdominopelvic								
With IV contrast agent								
< 8 kg	80	690	1.4	0.28	128 × 0.6	B40, I30–3	3/3	Varies (≈ 2.2)
8–20 kg	100	330	1.4	0.28	128 × 0.6	B40, I30–3	3/3	Varies (≈ 3.6)
20–45 kg	120	180	1.4	0.28	128 × 0.6	B40, I30–3	3/3	Varies (≈ 5.2)
Without IV contrast agent, 0–45 kg	120	180	1.4	0.28	128 × 0.6	B40, I30–3	33	Varies (≈ 4)
Chest								
With IV contrast agent								
< 8 kg	80	340	1.4	0.28	128 × 0.6	B40, I30–3	3/3	Varies (≈ 1.1)
8–20 kg	100	160	1.4	0.28	128 × 0.6	B40, I30–3	3/3	Varies (≈ 1.8)
20–45 kg	120	90	1.4	0.28	128 × 0.6	B40, I30–3	3/3	Varies (≈ 2.6)
Without IV contrast agent, 0–45 kg	120	90	1.4	0.28	128 × 0.6	B40, I30–3	3/3	Varies (≈ 2)

Note—$CTDI_{vol}$ = volume CT dose index.

AJR Am J Roentgenol. Author manuscript; available in PMC 2016 April 28.

TABLE 2

Patient and Dose Information for the 25 Abdominopelvic and 25 Chest CT Examinations Evaluated

CT Examination, Contrast Agent Status, Kilovoltage	No. of Patients	Age (y)		$CTDI_{vol}$ (mGy), Mean ± SD	SSDE (mGy), Mean ± SD
		Mean ± SD	Range		
Abdominopelvic					
With contrast agent					
80 kV	0	NA	NA	NA	NA
100 kV	11	8.4 ± 5.8	1–17	5.2 ± 2.5	9.1 ± 3.3
120 kV	13	9.6 ± 4.1	4–16	7.4 ± 5.6	11.1 ± 4.5
Without contrast agent, 120 kV	1	8.0 ± 0.0	8–8	4.0 ± 0.0	7.4 ± 0.0
Total	25	8.7 ± 4.8	1–17	6.4 ± 4.3	10.3 ± 3.8
Chest					
With contrast agent					
80 kV	1	0.0 ± 0.0	0–0	1.1 ± 0.0	2.6 ± 0.0
100 kV	8	2.0 ± 0.7	1–3	2.1 ± 0.6	4.5 ± 1.3
120 kV	4	7.2 ± 2.3	6–11	2.8 ± 0.7	5.1 ± 1.3
Without contrast agent, 120 kV	11	6.8 ± 5.7	1–17	2.6 ± 1.5	4.5 ± 1.8
Total	25	5.1 ± 4.7	0–17	2.4 ± 1.1	4.5 ± 1.5

Note—The volume CT dose index ($CTDI_{VOl}$) was based on a 32-cm CT dose index (CTDI) phantom. SSDE = size-specific dose estimate, NA = not applicable.

TABLE 3

Percentage Agreement Between Organ- and Structure-Specific Diagnosis Codes From the Three Half-Dose Configurations and the Full Dose Plus Filtered Back-Projection (FBP) Configuration in CT Examinations of Three Abdominopelvic Organs (Liver, Kidney, and Small Bowel)

Organ, Reader	Absolute Agreement, % (No./Total)			Normality Agreement, % (No./Total)		
	FBP	SAFIRE	aNLM	FBP	SAFIRE	aNLM
Liver						
Reader 1	80 (20/25)	92 (23/25)	92 (23/25)	88 (22/25)	92 (23/25)	96 (24/25)
Reader 2	92 (23/25)	96 (24/25)	100 (24/24)	96 (24/25)	100 (25/25)	100 (24/24)
Reader 3	92 (23/25)	88 (22/25)	88 (22/25)	92 (23/25)	88 (22/25)	88 (22/25)
All readers	88 (66/75)	92 (69/75)	93 (69/74)	92 (69/25)	93 (70/75)	95 (70/74)
Kidney						
Reader 1	88 (22/25)	76 (19/25)	96 (24/25)	100 (25/25)	84 (21/25)	100 (25/25)
Reader 2	96 (24/25)	96 (24/25)	96 (24/25)	96 (24/25)	96 (24/25)	96 (24/25)
Reader 3	100 (25/25)	92 (23/25)	100 (25/25)	100 (25/25)	92 (23/25)	100 (25/25)
All readers	95 (71/75)	88 (66/75)	97 (73/75)	99 (74/75)	91 (68/75)	99 (74/75)
Small bowel						
Reader 1	88 (22/25)	88 (22/25)	88 (22/25)	96 (24/25)	92 (23/25)	96 (24/25)
Reader 2	96 (23/24)	100 (24/24)	96 (23/24)	100 (24/24)	100 (24/24)	100 (24/24)
Reader 3	72 (18/25)	72 (18/25)	83 (20/24)	84 (21/25)	84 (21/25)	83 (20/24)
All readers	85 (63/74)	86 (64/74)	89 (65/73)	93 (69/74)	92 (68/74)	93 (68/73)

Note—The three half-dose configurations were FBP, sinogram-affirmed iterative reconstruction (SAFIRE, Siemens Healthcare), and adaptive nonlocal means (aNLM). Absolute agreement was the percentage of cases with absolute agreement between diagnosis codes. Normality agreement occurred if both the full-dose and the half-dose configurations were normal or if both were not normal.

TABLE 4

Percentage Agreement of Organ- and Structure-Specific Diagnosis Codes From the Three Half-Dose Configurations and the Full Dose Plus Filtered Back-Projection (FBP) Configuration in Two Chest Organs (Lung and Mediastinum).

Organ, Reader	Absolute Agreement, % (No./Total)			Normality Agreement, % (No./Total)		
	FBP	SAFIRE	aNLM	FBP	SAFIRE	aNLM
Lung						
Reader 1	88 (22/25)	84 (21/25)	80 (20/25)	96 (24/25)	92 (23/25)	92 (23/25)
Reader 2	96 (24/25)	100 (25/25)	100 (25/25)	96 (24/25)	100 (25/25)	100 (25/25)
Reader 3	84 (21/25)	92 (23/25)	92 (23/25)	84 (21/25)	92 (23/25)	92 (23/25)
All readers	89 (67/75)	92 (69/75)	91 (68/75)	92 (69/75)	95 (71/75)	95 (71/75)
Mediastinum						
Reader 1	100 (25/25)	96 (24/25)	100 (25/25)	100 (25/25)	96 (24/25)	100 (25/25)
Reader 2	96 (24/25)	96 (24/25)	100 (25/25)	96 (24/25)	96 (24/25)	100 (25/25)
Reader 3	88 (22/25)	92 (23/25)	92 (23/25)	88 (22/25)	92 (23/25)	92 (23/25)
All readers	95 (71/75)	95 (71/75)	97 (72/75)	95 (71/75)	95 (71/75)	97 (73/75)

Note—The three half-dose configurations were FBP, sinogram-affirmed iterative reconstruction (SAFIRE, Siemens Healthcare), and adaptive nonlocal means (aNLM). Absolute agreement was the percentage of cases with absolute agreement between diagnosis codes. Normality agreement occurred if both the full-dose and the half-dose configuration were normal or if both were not normal.